*Progress In Electromagnetics Research, Vol. 161, 101–111, 2018*

# Photo-Induced Electromagnetic Band Gap Structures for Optically Tunable Microwave Filters

**Jun Ren, Zhenguo Jiang, Md. Itrat Bin Shams, Patrick Fay, and Lei Liu***

**Abstract**—Electromagnetic band gap (EBG) structures offer unique solutions for effectively manipulating electromagnetic waves over a broad range of frequencies for a wide range of applications. However, most EBG designs reported so far either require sophisticated fabrication processes or have limited tunability and reconfigurability. In this paper, we investigate the potential to implement high performance tunable and reconfigurable EBG components using a novel optical control approach. This technology allows the generation of EBG structures through spatially-resolved photogeneration of free carriers in a semiconductor, without any complex fabrication processes. As a prototype demonstration, a reconfigurable microwave frequency tunable band-stop filter (BSF) based on photo-induced uniplanar EBG structures has been investigated through simulation. In this approach, the required EBG patterns are directly illuminated onto a Ge ground plane mounted to the bottom of a Duroid substrate for tunability using a digital light processing (DLP) projector. On the basis of HFSS simulations, the bandwidth of the BSF can be tuned by modifying the EBG pattern filling factor. The center frequency of the BSF could also be tuned from 8–12 GHz by adjusting the period of the EBG structure. In addition, two limiting factors, i.e., localized heating effects and finite lateral spatial resolution (due to carrier diffusion), that may affect the circuit performance in this technology have been investigated and discussed. By using a mesa-array structured ground plane, this approach is promising for developing tunable and reconfigurable circuits such as filters from the microwave to terahertz regimes.

## 1. INTRODUCTION

Periodic structures have been extensively studied and employed for a variety of microwave applications including filters, resonators, power amplifiers, travelling-wave tubes, frequency-selective surfaces, and phased array antennas [1–9]. They have also been adopted as building blocks to improve the overall circuit performance, such as facilitating broadband and high gain performance of hemispherical dielectric resonators, and augmenting radiation losses and roll-off factor of spur line resonator based low pass filters [10–12]. Around two decades ago, Yablonovitch and his colleagues demonstrated a 3-D periodic structure operating at microwave frequencies by mechanically drilling holes into a block of dielectric material [1, 2]. Although the dielectric material in its solid form is transparent at those frequencies, the resulting structure prohibits the propagation of waves in certain frequency bands. Such wave propagation band gaps are generated by introducing periodic changes in dielectric properties on a length scale comparable to the wavelength, resulting in a dispersion diagram similar to those in periodic semiconductor lattices [2]. This kind of artificially engineered material is generally known as either photonic band gap (PBG) materials (in the photonics community) or electromagnetic band gap (EBG) materials (in the microwave community) [3]. Due to the fact that EBG structures can be used to guide and efficiently control the propagation of electromagnetic waves to an extent that was previously not possible, they have become one of the most rapidly advancing topics in microwave engineering [3–12].

*Received 3 December 2017, Accepted 8 April 2018, Scheduled 18 April 2018*
* Corresponding author: Lei Liu (Liu_Lei@nd.edu).
The authors are with the Department of Electrical Engineering, University of Notre Dame, Notre Dame, IN, 46556, USA.

Despite the success in implementing EBG structures for microwave applications, most current EBG designs either require sophisticated fabrication processes such as silicon micromachining or combinations of wet- and dry-etching to create structures with strong material property contrast [7, 8], or have very limited tunability or reconfigurability. Because the frequency responses of an EBG rely on the contrast between the materials involved, circuit tunability and reconfigurability are challenging to realize since at least one of the materials' dielectric properties must be dynamically adjusted. The conventional approach is to use either electrical tuning using PIN diodes as varactors or mechanical deformation of MEMS (micro electro mechanical systems) devices. Both of these approaches typically result in complex systems with limited tuning capability [13, 14]. To overcome these drawbacks, alternative design strategies are needed.

In this paper, we investigate the performance potential of tunable and reconfigurable EBG components using a novel optical control methodology [15–18]. This approach is based on the generation of EBG structures through spatially-resolved photogeneration of free carriers in a semiconductor, without the need for complex fabrication processes. Tunability is realized by illuminating different virtual EBG patterns onto the semiconductor. Although optical tuning has been studied for implementing tunable circuits using optical fiber bundle arrays or switchable LEDs [19, 20], the approach described in this paper is considerably more flexible and can be used to achieve dynamic, reconfigurable, and multifunctional circuits. For a prototype demonstration, the EBG structures evaluated here are based on a microstrip line configuration with the ground plane replaced by a semiconductor that can be selectively patterned using optical generation. The optical patterns illuminating the ground are used to generate uniplanar EBG structures [4] by spatially modulating the photogenerated free carriers in the ground plane. A commercially available digital light processing (DLP) projector is used to project these patterns onto the ground plane. On the basis of this basic structure, a tunable and reconfigurable microwave band-stop filter (BSF) operating in the frequency range from 8–12 GHz has been designed and studied. HFSS simulations show that both the bandwidth and the center frequency of the BSF can be tuned by modifying the ground plane EBG pattern filling factor and period, respectively. In addition, two limiting factors, localized heating effects and finite lateral spatial resolution (due to carrier diffusion), that may affect the circuit performance in this technology have been investigated and discussed. By using a mesa-array structured ground plane, this approach is promising for developing tunable and reconfigurable circuits such as filters from the microwave to terahertz regimes.

## 2. PROPOSED STRUCTURE FOR PHOTO-INDUCED EBG COMPONENT

Figure 1 illustrates the cross-sectional view of the structure evaluated here for implementing photo-induced tunable and reconfigurable EBG components. The structure is based on a microstrip line configuration with the top conductor fabricated on a dielectric substrate. The back conductor is partially removed and replaced by a semiconductor film (e.g., Si, Ge, etc.) to facilitate optically-modulated conductivity. When the semiconductor is illuminated, free carriers are generated as long as the photon energy is larger than the semiconductor band gap. Therefore the material properties of the illuminated region, such as complex relative permittivity and conductivity, can be controlled optically [21, 22]. By projecting different periodic patterns onto the semiconductor back plane using a DLP projector, uniplanar EBG configurations with tunable properties can be achieved. As a result, electromagnetic waves propagating along the microstrip line are perturbed by the photo-induced EBG structures, leading to the potential for dynamic tuning and reconfigurability. The theory of operation for this type of device is discussed in the following section.

## 3. THEORIES AND MECHANISMS OF PHOTO-INDUCED EBG

To understand the mechanism of operation for the proposed EBG structures, we first consider the optical control of the conductivity of a thin semiconductor film. For a semiconductor wafer with a thickness of $h$ and uniform optical excitation normally incident on its surface, photo-induced excess (free) carriers are created in the semiconductor as long as the incident photon energy is higher than the semiconductor band gap. The generation rate of the free carriers decays exponentially along the direction of optical propagation (denoted as $z$, see Fig. 1) and is determined by the illumination intensity, the

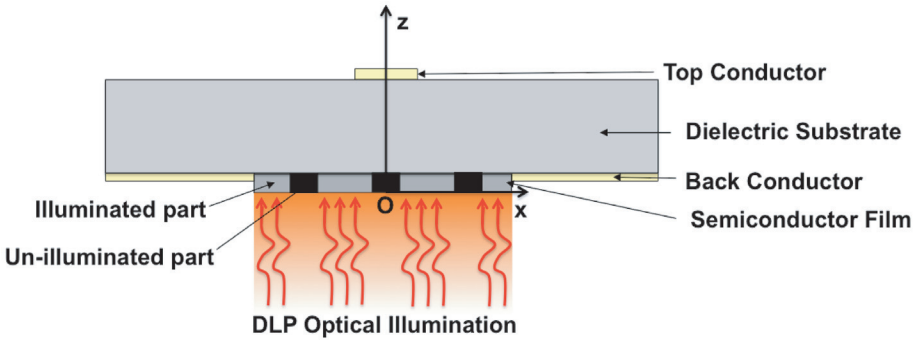


**Figure 1.** Cross-sectional view of the proposed structure for implementing optically-controlled tunable and reconfigurable uniplanar EBG component in a microstrip line configuration. Virtual EBG patterns are projected onto the semiconductor film using a DLP projector to form uniplanar EBG configuration with tunable properties.

reflectivity of the wafer, and the absorption coefficient of the semiconductor at the optical illumination wavelength. Under the assumption that surface recombination effects are negligible (e.g., with suitable surface passivation [23]), the photo-excited free carrier concentration profile can be calculated by solving the continuity equation. In the absence of externally-applied bias, the photogenerated electron-hole pairs are bound together through Coulombic interaction, leading to an ambipolar response. In this case, the concentration of photogenerated electron-hole pairs, $N(z)$, as a function of depth into the wafer can be written as [15]:

$$N(z) = \frac{\tau_e \alpha P_0 (1-R)}{\hbar\omega} \frac{1}{1-(\alpha L_D)^2} \left[ e^{-\alpha z} - \alpha L_D \left( e^{-z/L_D} \left( \frac{1-e^{-(\alpha+1/L_D)h}}{1-e^{-2h/L_D}} \right) - e^{z/L_D} \left( \frac{1-e^{-(\alpha-1/L_D)h}}{1-e^{2h/L_D}} \right) \right) \right] \quad (1)$$

where $\tau_e$ is the effective carrier lifetime, $\alpha$ the absorption coefficient of the semiconductor at the illumination wavelength, $P_0$ the light intensity, $\omega$ the angular frequency of the light, $\hbar$ the reduced Planck constant, $R$ the reflectivity of the wafer, and $L_D$ the ambipolar diffusion length calculated using the diffusion characteristics of both electrons and holes [25]. Once the free carrier distribution inside the wafer is determined, the corresponding photoconductivity profile can be calculated using:

$$\sigma(z) = qN(z)(\mu_e + \mu_h) \quad (2)$$

where $q$ is the elementary charge, and $\mu_e$ and $\mu_h$ are the mobility of electrons and holes, respectively. This physics-based model for photoconductivity has been previously applied to the study of THz wave modulation depth [15–18]. Since the photoconductivity of the semiconductor can be controlled by the incident illumination, as shown in Eqs. (1) and (2), a desired spatial distribution of the photoconductivity can be generated by employing patterned light (so that certain areas of the wafer are photo-excited, while others are not). This photo-induced spatial modulation strategy allows for the formation of periodic structures in the semiconductor without any complex fabrication processes, and therefore offers a simple but powerful approach for the implementation of tunable and reconfigurable EBG components.

For realizing EBG structures using spatially-resolved photogenerated free carriers, a sufficiently high free carrier concentration needs to be created in the illuminated excited areas so that a strong conductivity contrast can be established between illuminated and un-illuminated regions. This is the central challenge associated with the proposed approach. The key factors that determine the conductivity contrast include the choice of semiconductor material, wafer thickness, and light intensity.

With respect to material selection for efficient spatially-resolved optical modulation, a detailed assessment among three mainstream semiconductors (Si, Ge, and GaAs) was recently investigated [15]. It is found that in addition to mobility, effective carrier lifetime of the photoconductive semiconductor

is the key parameter for determining the modulation strength. Among the three candidates evaluated, Ge provides the highest free carrier concentration under the same light intensity with wavelengths in the visible range (e.g., 550 nm) owing to its long effective carrier lifetime (typically 10 times larger than that of Si, and $10^5$ times that of GaAs), while still offering excellent electron and hole mobilities (roughly of the same order of magnitude as that of the other two materials). As a consequence, Ge is chosen for the device explored here as it can provide a high free carrier density at moderate light intensity.

Wafer thickness and light intensity are also critical in controlling device performance. The impact of these factors on the photoconductivity profile (along the $z$ direction) for several wafer thicknesses (i.e., 25 μm, 50 μm, 100 μm, 250 μm, and 500 μm, respectively) was calculated using Eqs. (1) and (2). In this calculation, light with a wavelength of 550 nm was employed. The calculation was repeated for incident light with different light intensities, i.e., 2 W/cm$^2$, 20 W/cm$^2$, and 200 W/cm$^2$, respectively. The physical parameters used for the calculation are tabulated in Table 1. The parameters in the table are standard values from the literature [24, 25], except for effective carrier lifetime and the corresponding diffusion length. On the basis of THz transmission measurements of a Ge wafer ($\sim$ 500 μm thick), which have shown a maximum modulation depth of 65 dB using a 4.2 W/cm$^2$ light intensity [23], the actual lifetime for the Ge wafer to be employed in our work was estimated to be approximately 40 μs (values from the literature are typically larger, which may result in better performance). To be conservative, the lower value of 40 μs has been taken here. Fig. 2(a) shows the photoconductivity as a function of depth into the Ge for different thicknesses under the same light intensity (2 W/cm$^2$). The photoconductivity profile for each thickness has been normalized to its peak value. It can be observed that the photoconductivity profile is characterized by a decreasing of photoconductivity with increasing depth, but the variation is small because the wafer thickness is below or (at most) equal to the ambipolar diffusion length ($\sim$ 500 μm). These results show that for $h < L_D$, the photoconductivity distribution is nearly homogenous, allowing one to model the wafer as a single optically excited semiconductor layer with a conductivity equal to the spatially averaged value. The spatially averaged photoconductivity as a function of wafer thickness and light intensity is shown in Fig. 2(b). It can be seen that: (1) for a given wafer thickness, higher light intensity leads to higher photoconductivity; (2) under the same light intensity, thinner wafers show higher photoconductivity as there is limited space available in the semiconductor for the photo-excited free carriers to diffuse. These two observations indicate that both stronger light intensity and thinner wafers lead to higher photoconductivity. As an example, for a Ge wafer with $\sim$ 100 μm thickness, $\sim$ 20 W/cm$^2$ light intensity (which can be readily provided by a commercially available DLP projector [17]) would lead to a photoconductivity of the order of $10^4$ S/m, while over 200 W/cm$^2$ light intensity (which can be implemented by using a high power DLP projector, or using a high power laser diode in conjunction with a DMD chip [18]) would yield a photoconductivity of the order of $10^5$ S/m. When high light intensity is required, heating effects may need to be considered in practice to ensure circuit stability and reliability. The impact of local heating will be discussed later in this paper. The use of thinner Ge wafers relieves the requirement on light intensity for achieving the same level of photoconductivity, thereby reducing the need for cooling while still maintaining the same level of circuit performance. However, it should be noted that even though employing thinner wafer and stronger light intensity can both yield higher photoconductivity, reducing the wafer thickness does not always provide improved photo-induced spatial modulation (as increasing the light intensity

**Table 1.** Material parameters of Ge at room temperature [24, 25].

| | **Description** | **Value** |
|---|---|---|
| $\alpha$ | Absorption coefficient at 550 nm optical illumination | $5.03 \times 10^5\,\mathrm{cm}^{-1}$ |
| $D_a$ | Ambipolar diffusion coefficient | $63.88\,\mathrm{cm}^2/\mathrm{s}$ |
| $\tau_e$ | Effective carrier lifetime | $40 \times 10^{-6}\,\mathrm{s}$ |
| $L_D$ | Ambipolar diffusion length | $5.05 \times 10^{-2}\,\mathrm{cm}$ |
| $\mu_e$ | Electron mobility | $3900\,\mathrm{cm}^2/\mathrm{Vs}$ |
| $\mu_h$ | Hole mobility | $1900\,\mathrm{cm}^2/\mathrm{Vs}$ |

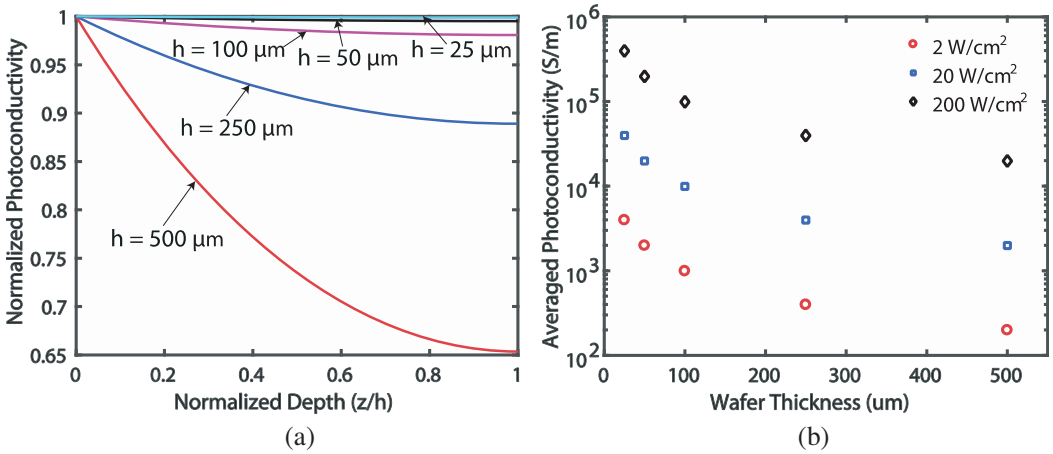


**Figure 2.** (a) Normalized photoconductivity as a function of depth into Ge for different wafer thicknesses (i.e., 25 μm, 50 μm, 100 μm, 250 μm and 500 μm, respectively) illuminated by continuous 550 nm light. (b) Spatially averaged photoconductivity in Ge as a function of wafer thickness and light intensity (i.e., 2 W/cm$^2$, 20 W/cm$^2$, and 200 W/cm$^2$, respectively).

does) because aggressively thinning down the wafer (while keeping the same light intensity) may lead to the situation where the skin depth is comparable or even larger than the wafer thickness. This is especially true at lower frequencies and under low light intensities. For achieving efficient photo-induced spatial modulation, the thickness of the wafer should be several times the skin depth at the operation frequency.

## 4. PHOTO-INDUCED EBG FILTER DESIGN, SIMULATION, AND ANALYSIS

The proposed photo-induced EBG configuration can be used as a platform to design a variety of tunable and reconfigurable circuits (e.g., filters, resonators) with multiple functionalities. The operation of those circuits takes advantage of the stop-band phenomenon in EBG structures. Such a stop-band phenomenon for electromagnetic waves propagating in EBG structures can be understood in analogy to the movement of free electrons in semiconductor lattice [25]. The electrons will experience the periodicity of the lattice in the form of an electrostatic periodic potential while moving through the semiconductor crystal. According to the perturbation theory, this will lead to energy discontinuities at the edges of the Brillouin zone ($k = \pm\pi/a$, where $k$ is the wave vector, and $a$ is the periodicity of the lattice). By analogy, the electromagnetic waves propagating inside an EBG structure will be modulated by the periodic change of material properties, and therefore exhibit a stop-band at around the frequency where the condition $k = \pm n\pi/a$ ($n$ is an integer) is satisfied. This condition corresponds to $a = \pm n\lambda_g/2$, where $\lambda_g$ is the guided wavelength in the wave propagating medium [26–29]. As a prototype demonstration, an X-band microwave BSF with a tunable center frequency has been designed using the uniplanar EBG structures reported in [4]. As illustrated in Fig. 3(a), the circuit is made using a 50-mil thick dielectric substrate with a dielectric constant of 10.2 and loss tangent of 0.0023 (e.g., Rogers RT/Duroid 6010 [30]). The size of the substrate is 10 cm × 5 cm, and the width of the top conductor (copper) is 1.19 mm (corresponding to the top conductor width of a 50-Ohm line in conventional microstrip). At the backside of the substrate, the conventional ground plane is removed from a rectangular area with a dimension of 22 mm × 20 mm and replaced by a 100-μm thick undoped Ge thin film of the same size. A thickness of 100 μm is chosen for the semiconductor film because it facilitates obtaining relatively high photoconductivity under moderate light intensity while maintaining ease of handling in practice. EBG patterns were imposed onto the Ge thin film (e.g., using a DMD chip from a DLP projector). A representative photo-induced uniplanar EBG pattern for a BSF with a 10 GHz center frequency is shown in Fig. 3(b). It consists of three rows of circles with a radius, $r$, of 2.28 mm, arranged in four columns with a period, $a$, of 5.7 mm, corresponding to half of the guided wavelength at 10 GHz. The dark areas correspond to the intrinsic dielectric regions without illumination. For full wave

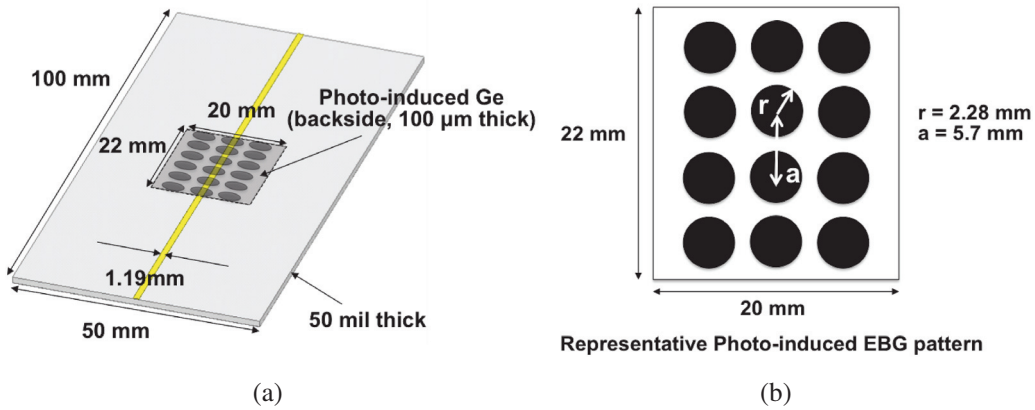


**Figure 3.** Depiction of a microwave filter design based on photo-induced uniplanar EBG structures: (a) perspective view of the circuit, and (b) representative photo-induced uniplanar EBG pattern.

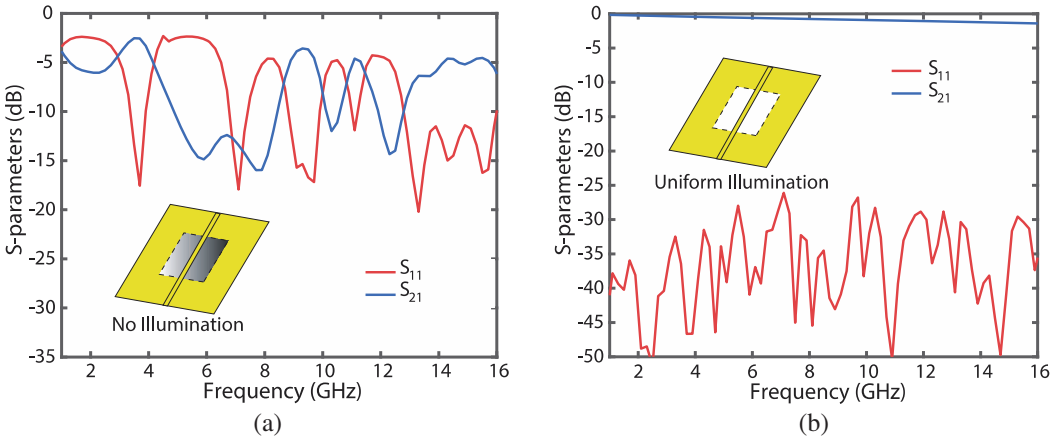


**Figure 4.** Simulated $S$-parameters of the microstrip line (a) without optical illumination and (b) with uniform optical illumination (200 W/cm$^2$).

simulation, homogeneous cylinders with the conductivity of intrinsic Ge (i.e., 2 S/m, data supplied by the wafer manufacturer) were used to model the un-illuminated regions, while materials with uniform photoconductivity determined by the incident light intensity (as computed using Eqs. (1) and (2)) were employed to model the illuminated parts (white areas in Fig. 3(b)).

To verify the effectiveness of the proposed optical modulation approach, HFSS simulation (ANSYS HFSS version 18.0) of the circuit frequency responses without optical illumination was first investigated; Fig. 4(a) shows the simulated $S$-parameters in the frequency range from 1–16 GHz. The simulated return loss oscillates significantly from 3 dB to 20 dB (due to the standing wave effect caused by the discontinuities introduced by the Ge thin film on the ground plane) and the insertion loss is larger than 4 dB over the entire frequency range, indicating that the quasi-TEM mode cannot propagate along the transmission line due to the presence of intrinsic Ge with poor conductivity on the ground. However, when the Ge slab is uniformly illuminated at an optical intensity of 200 W/cm$^2$, a return loss well above 20 dB and an insertion loss less than 1.5 dB are observed across the entire frequency range as seen in Fig. 4(b). This is because sufficient free carriers have been generated to produce a conductivity in the Ge approaching $\sim 1 \times 10^5$ S/m (see Fig. 2(b)). The corresponding skin depth at $\sim$ 10 GHz is $\sim$ 15 μm, and the wafer thickness is more than 6 times that of the skin depth. As a result, the photo-excited Ge shows metallic behavior and serves as a ground plane to support the propagation of quasi-TEM mode in the microstrip structure. Consequently, a typical transmission line response is observed.

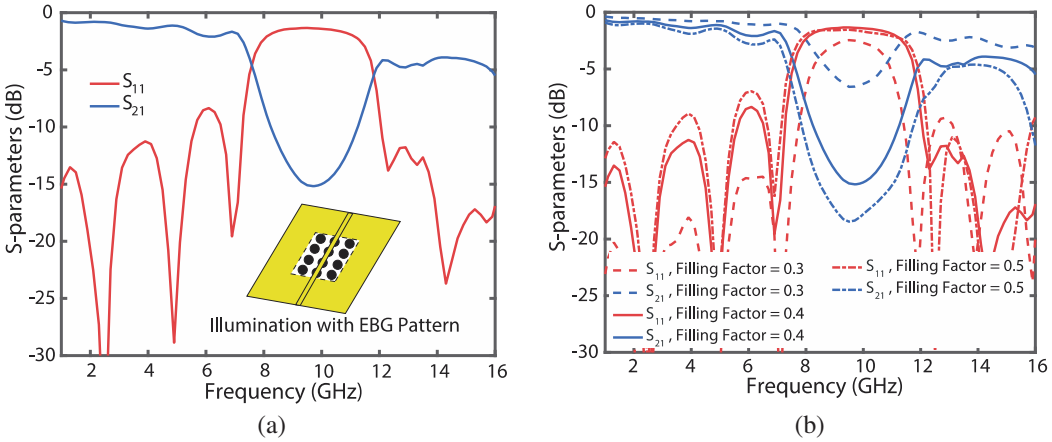


**Figure 5.** (a) Simulated $S$-parameters of the prototype BSF with an EBG photo-induced pattern (as illustrated in Fig. 3(b)). (b) Simulated $S$-parameters of the prototype with three different EBG photo-patterns with fixed period of 5.7 mm but different filling factor (0.3, 0.4, and 0.5, respectively).

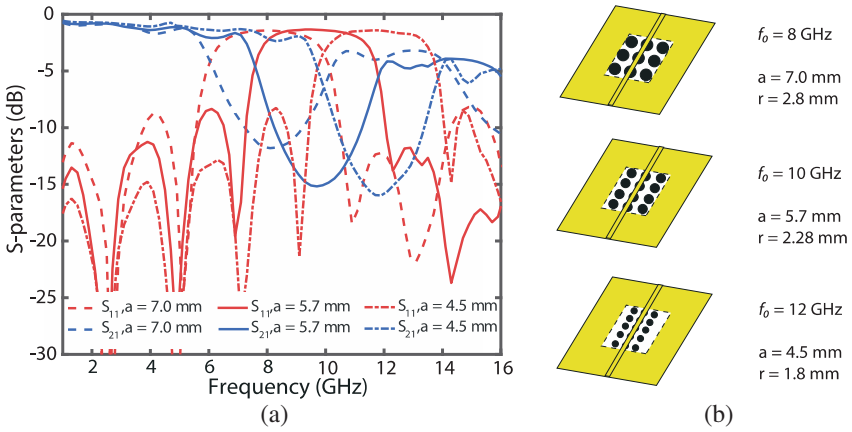


**Figure 6.** (a) Simulated $S$-parameters of the tunable BSF prototype in response to (b) EBG photo-patterns with various periods.

To realize a BSF with this structure, the Ge is illuminated with an EBG optical pattern as depicted in Fig. 3(b). Fig. 5(a) shows the simulated $S_{11}$ and $S_{21}$. This simulation was performed with a light intensity of 200 W/cm$^2$, corresponding to a photoconductivity of $1 \times 10^5$ S/m. As seen in Fig. 5(a), BSF responses with a center frequency $f_0$ at 10 GHz, a stop-band rejection of $\sim 15$ dB and sharp roll-off have been obtained. The filling factor $(r/a)$ of the photo-induced EBG pattern used in Fig. 3(b) is 0.4. To investigate how the filling factor affects the filter performance and to demonstrate the flexibility of this approach, frequency responses using three different photo-induced EBG patterns with fixed period ($a = 5.7$ mm) but different filling factors (0.3, 0.4, and 0.5, respectively) were simulated and plotted in Fig. 5(b). In all three cases, the stop-band is centered at 10 GHz, due to the fixed EBG period. However, both the depth and bandwidth of the stop-band can be adjusted by modifying the EBG pattern filling factor. Use of a large filling factor results in increased stop-band rejection and bandwidth, but leads to significant insertion loss in the pass-band. Conversely, smaller filling factor leads to reduced pass-band insertion loss but smaller stop-band rejection. Note that if the filling factor is modified by changing the period while remaining the radius, then the center frequency of the stop-band will no longer be fixed at 10 GHz. Tuning of the center frequency will be discussed as follows.

Tuning of the center frequency can be accomplished by changing the period of the photo-induced EBG patterns. To demonstrate this, the period of the photo-induced EBG patterns was varied from

4.5 mm to 7 mm. The radius of the circles was scaled proportionally to remain a filling factor of 0.4. The simulated $S$-parameters with different periods are shown in Fig. 6(a) for the EBG patterns illustrated in Fig. 6(b). As can be seen, the center frequency $f_0$ is tuned from 8 GHz to 12 GHz as the EBG period is varied, consistent with expectations. The stop-band rejection exceeds 12 dB in all cases, and the return loss in the stop-band is less than 1.5 dB. This demonstration shows that broad tunability can be easily achieved using the proposed photo-induced EBG approach. We note that the approach is not limited to band-stop filters; other tunable and reconfigurable circuits such as band-pass filters and resonators can also be realized by modifying the EBG patterns [8, 31–33].

Although satisfactory performance has been demonstrated from these simulations, there are two limiting factors for this technology that may affect the circuit performance significantly in practice. The first is the impact of localized heating. Due to the use of optical intensities of up to 200 W/cm$^2$, the temperature of the semiconductor wafer (i.e., Ge in this work) for EBG pattern illumination may change. As a result, the carrier concentration (and hence the photoconductivity) in un-illuminated areas will increase due to the increase in intrinsic carrier concentration with temperature. To overcome this problem, effective thermal management needs to be employed to ensure circuit stability and reliability. Solutions for cooling such as heat sinks and thermoelectric coolers have been proposed and discussed in the literature [34–36]. An alternative approach for solving the heating issue is to employ even thinner Ge film. It can be speculated from Fig. 2(b) that a photoconductivity of the order of $10^5$ S/m can also be achieved under a much lower light intensity of $\sim 50$ W/cm$^2$ by using a 25 μm Ge on the same RT/Duroid substrate. Comparable circuit performance can be expected (or at most with moderate degradation in terms of the loss performance as the skin depth now is $\sim 60\%$ of the wafer thickness due to the reduction of the wafer thickness), but the heating effects would be reduced with a much lower light intensity employed.

The second limiting factor is the finite lateral spatial resolution determined by carrier diffusion in Ge. In the EBG structure design discussed above, a simplified model that assumes no free carrier lateral diffusion was used. In reality, photogenerated carriers will inevitably diffuse across the boundary of the illuminated and un-illuminated regions. The free carriers that diffuse out of the illuminated areas both lower the photogenerated carrier concentration as well as expand the effective size of the photoconductive patterns, with a size scale comparable to the ambipolar diffusion length. This imposes significant limits on the spatial resolution of the photo-induced EBG patterns. In the X-band prototype design discussed here this is a minor effect because the diffusion length in Ge ($\sim 0.5$ mm) is only about 1/10 of that of the smallest feature size of the photo-induced EBG pattern ($\sim 5$ mm), and this effect can be compensated for (within limits) by adjusting the size of the projected EBG features.

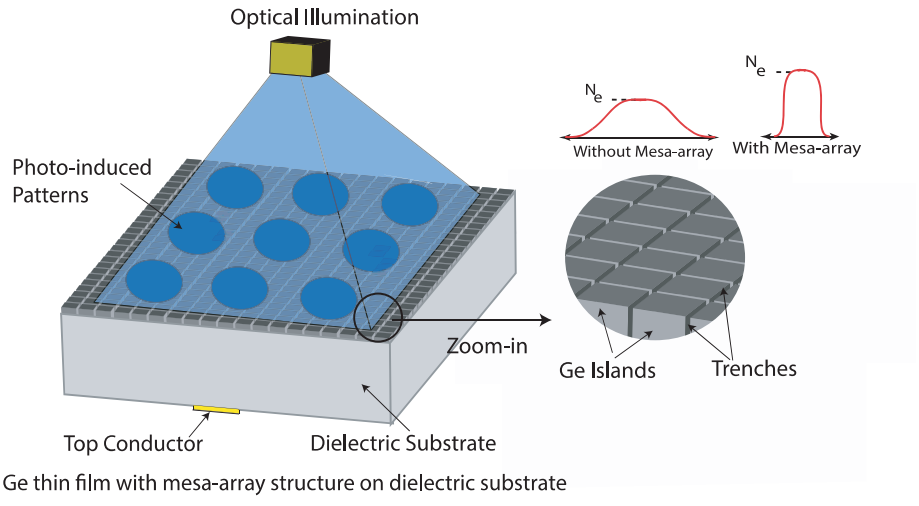


**Figure 7.** Illustration of a Ge-based mesa-array structure on a dielectric substrate. The mesa-array structure consists of a matrix of Ge islands. Each island is electrically isolated to prevent lateral diffusion, and the dimensions are much smaller than either the wavelength or the carrier diffusion length.

To circumvent this problem and enable spatial resolution at or below the diffusion length limit, the lateral diffusion of free carriers in Ge can be controlled by using an artificially constructed mesa-array structure. Fig. 7 conceptually illustrates a Ge mesa-array structure employed for photo-induced EBG component design. The mesa-array structure is made of a matrix of electrically-isolated islands, the dimension of which can be made much smaller than both the microwave wavelength and the carrier diffusion length by using deep reactive ion etching. When such an artificially engineered structure is optically illuminated, the photogenerated carriers are confined within each isolated mesa. Carrier diffusion from one island to another is eliminated by the mesa sidewall isolation, and therefore much higher spatial resolution can be achieved even in materials with large diffusion lengths. As an example, simulations have been performed on a 5 µm thick Ge mesa-array with cell size of 4.75 µm × 4.75 µm separated by 0.5 µm wide trenches [15]. It is shown that 10 µm resolution has been achieved using the proposed mesa-array structure. Such a structure can be fabricated using a process described in [37]. With the much-improved spatial resolution, the presented design methodology for implementing tunable and reconfigurable microwave circuits can be extended to higher frequencies, potentially to the THz domain.

## 5. CONCLUSIONS

In this work, a simple but powerful optically-controlled tuning methodology for implementing high performance tunable and reconfigurable EBG components using spatially-resolved photogeneration of free carriers in a semiconductor is proposed. A reconfigurable microwave circuit with tunable BSF responses from 8–12 GHz was designed based on photo-induced uniplanar EBG structures as a prototype demonstration to verify the effectiveness of the proposed optical modulation approach. HFSS simulations have shown that important characteristics of the BSF, such as the stop-band bandwidth and the center frequency, can be tuned by changing the EBG patterns illuminated on the Ge ground plane. Two limiting factors, including localized heating and finite lateral spatial resolution of the photo-induced patterns in Ge, that may affect the circuit performance in this technology have also been investigated and discussed. By using a mesa-array technique, it is expected that the optical control methodology proposed in this work can be used to design high performance tunable/reconfigurable circuits such as filters from microwave to THz frequencies.

## ACKNOWLEDGMENT

This work is partially supported by the National Science Foundation (NSF) under the grant of ECCS-1711631 and ECCS-1711052, and a subcontract from the Harvard-Smithsonian Center for Astrophysics under grant PTX-Smithsonian 17-SUBC-400SV787007. The authors would like to thank the support from Notre Dame's Center for Nano Science and Technology (NDnano) and Advanced Diagnostics & Therapeutics (AD&T) at the University of Notre Dame.

## REFERENCES

1. Yablonovitch, E., "Inhibited spontaneous emission in solid-state physics and electronics," *Phys. Rev. Lett.*, Vol. 58, 2059, 1987.
2. Yablonovitch, E. and T. J. Gmitter, "Photonic band structure: The face-centered-cubic case," *Phys. Rev. Lett.*, Vol. 63, 18, 1989.
3. Oliner, A. A., "Periodic structure and photonic band-gap terminology: Historical perspectives," *IEEE 29th European Microwave Conference*, Vol. 3, 295–298, 1999.
4. Radisic, V., Y. Qian, and T. Itoh, "Broad-band power amplifier integrated with slot antenna and novel harmonic tuning structure," *IEEE MTT-S Microwave Symp. Dig.*, 1895–1898, Baltimore, MD, June 7–12, 1998.
5. De Maagt, P., R. Gonzalo, J. Vardaxoglou, and J.-M. Baracco, "Electromagnetic bandgap antennas and components for microwave and (sub)millimeter wave applications," *IEEE Trans. Antennas and Propagation*, Vol. 51, No. 10, 2667–2677, 2003.

6. Chappell, W. J. and X. Gong, "Wide bandgap composite EBG substrates," *IEEE Trans. Antennas and Propagation*, Vol. 51, No. 10, 2744–2750, 2003.
7. Euler, T. and J. Papapolymerou, "Silicon micromachined EBG resonator and two-pole filter with improved performance characteristics," *IEEE Microwave and Wireless Components Lett.*, Vol. 13, No. 9, 373–375, 2003.
8. Hsu, H., M. J. Hill, R. W. Ziolkowski, and J. Papapolymerou, "A duroid-based planar EBG cavity resonator filter with improved quality factor," *IEEE Antennas and Wireless Propagation Lett.*, Vol. 1, No. 6, 67–70, 2002.
9. Fu, Y.-Q., G.-H. Zhang, and N.-C. Yuan, "A novel PBG coplanar waveguide," *IEEE Microwave and Wireless Components Lett.*, Vol. 11, No. 11, 447–449, 2001.
10. Mukherjee, B., V. D. Kumar, and M. Gupta, "A novel hemispherical dielectric resonator antenna on an electromagnetic band gap substrate for broadband and high gain systems," *AEU — International Journal of Electronics and Communication*, Vol. 68, 1185–1190, Elsevier, 2014.
11. Mukherjee, B., S. Tiwari, and A. L. Samariya, "Improvement in Radiation losses of Spur Line Resonators based LPF on an EBG substrate," *International Journal of Applied Electromagnetics and Mechanics*, Vol. 41, No. 4, 447–455, IOS Press, 2013.
12. Mukherjee, B., A. L. Samariya, and S. Tiwari, "Improvement in roll off factor of low pass filter placed on an EBG substrate," *Frequenz: Journal of RF Engineering and Telecommunications*, Vol. 67, Nos. 3–4, 73–78, February 2013.
13. Delustrac, A., F. Gadot, E. Akmansoy, and T. Brillat, "High-directivity planar antenna using controllable photonic bandgap material at microwave frequencies," *APhys. Lett.*, Vol. 78, 4196, 2002.
14. Mercier, L., M. Thevenot, P. Blonby, and B. Jecko, "Design and characterization of a smart periodic material including MEMS," *Proc. 27th ESA Antenna Technology Workshop on Innovative Periodic Antennas: Elecromagnetic Bandgap, Left-Handed Materials, Fractal and Frequency Selective Surfaces*, Santigao de Compostela, Spain, March 2004.
15. Kannegulla, A., M. I. B. Shams, L. Liu, and L.-J. Cheng, "Photo-induced spatial modulation of THz waves: Opportunities and limitations," *Opt. Exp.*, Vol. 23, No. 25, 32098–32112, 2015.
16. Kannegulla, A., et al., "Coded-aperture imaging using photo-induced reconfigurable aperture arrays for mapping terahertz beams," *IEEE Trans. THz Sci. Technol.*, Vol. 4, No. 3, 321–327, May 2014.
17. Shams, M. I. B., Z. Jiang, J. Qayyum, S. Rahman, P. Fay, and L. Liu, "A Terahertz reconfigurable photo-induced fresnel-zone-plate antenna for dynamic two-dimensional beam steering and forming," *International Microwave Symposium*, 1–4, Phoenix, Arizona, 2015.
18. Jiang, Z., M. I. B. Shams, L.-J. Cheng, P. Fay, J. L. Hesler, C. E. Tong, and L. Liu, "Investigation and demonstration of a WR-4.3 optically-controlled waveguide attenuator," *IEEE Trans. THz Sci. Technol.*, Vol. 7, No. 1, 20–26, 2017.
19. Platte, W., "LED-induced distributed Bragg reflection microwave filter with fiber-optically controlled change of center frequency via photoconductivity gratings," *IEEE Trans. Microwave Theory and Techniques*, Vol. 39, No. 2, 359–363, 1991.
20. Vardaxoglou, J. C., D. S. Lockyer, Y. L. R. Lee, and A. Chauraya, "Photonic bandgap and bandpass characteristics from metallodielectric periodic array structures," *Proc. 24th ESA Antenna Technology Workshop on Innovative Periodic Antennas: Elecromagnetic Bandgap, Left-Handed Materials, Fractal and Frequency Selective Surfaces*, Noordwijk, The Netherlands, June 2001.
21. Ulbricht, R., et al., "Carrier dynamics in semiconductors studied with time-resolved terahertz spectroscopy," *Rev. Modern Phys.*, Vol. 83, No. 2, 543–586, 2011.
22. Pierretand, R. F. and G. W. Neudeck, "Recombination-generation processes," *Advanced Semiconductor Fundamentals*, 2nd Edition, Vol. 6, 134–140, Addison-Wesley, Reading, MA, USA, 1987.
23. Liu, L., et al., "Tunable and reconfigurable THz devices for advanced imaging and adaptive wireless communication," *Proc. SPIE*, 9934, Terahertz Emitters, Receivers, and Applications VII, 993407, 2016.

24. Palik, E. D., *Handbook of Optical Constants of Solids*, Academia, 1988.
25. Sze, S. M., *Physics of Semiconductor Devices*, Wiley Publishers, 1981.
26. Koshiba, M., Y. Tsuji, and M. Hikari, "Time-domain beam propagation method and its application to photonic crystal circuits," *J. Lightwave Technol.*, Vol. 18, 102–110, 2000.
27. Koshiba, M., "Wavelength division multiplexing and demultiplexing with photonic crystal waveguide couplers," *J. Lightwave Technol.*, Vol. 19, 170–175, 2001.
28. Pendry, J. B. and A. MacKinnon, "Calculation of photon dispersion relations," *Phys. Rev. Lett.*, Vol. 69, 2772–2775, 1992.
29. Pendry, J. B., "Photonic band structures," *Journal of Modern Optics*, Vol. 41, 209–229, 1994.
30. http://www.rogerscorp.com/documents/612/index.aspx.
31. Hao, Z.-C., W. Hong, J.-X. Chen, and K. Wu, "Compact super-wide bandpass substrate integrated waveguide (SIW) filters," *IEEE Trans. Microwave Theory and Tech.*, Vol. 53, No. 9, September 2005.
32. Cassivi, Y. and K. Wu, "NRD-guide spurious mode suppressor using self-contained periodic planar EBG structure," *IEEE Proc. APMC*, 659–662, Taipei, 2001.
33. Gong, X., W. J. Chapper, and L. P. B. Katehi, "Reduced size capacitive defect EBG resonator," *IEEE MTT-S International Microwave Symposium Digest*, Vol. 2, 1091–1094, June 2002.
34. Tuckerman, D. B. and R. F. W. Pease, "High-performance heat sinking for VLSI," *IEEE Electron Device Letters*, Vol. edl-2, No. 5, 126–129, May 1981.
35. Chu, R. C., R. E. Simons, M. J. Ellsworth, R. R. Schmidt, and V. Cozzolino, "Review of cooling technologies for computer products," *IEEE Trans. Device and Materials Reliability*, Vol. 4, No. 4, 568–585, December 2004.
36. Bottner, H., J. Nurnus, A. Gavrikov, G. Kuhner, M. Jagle, C. Kunzel, D. Eberhard, G. Plescher, A. Schubert, and K.-H. Schlereth, "New thermoelectric components using microsystem technologies," *Journal of Microelectromechanical Systems*, Vol. 13, No. 3, 414–420, June 2004.
37. Lindblom, M., J. Reinspach, O. von Hofsten, M. Bertilson, H. M. Hertz, and A. Holmberg, "High-aspect-ratio germanium zone plates fabricated by reactive ion etching in chlorine," *J. Vac. Sci. Technol. B*, Vol. 27, No. 2, L1– L3, March/April 2009.